JACS
JOURNAL OF THE AMERICAN CHEMICAL SOCIETY

Article

pubs.acs.org/JACS

A Rationally Designed Upconversion Nanoprobe for *in Vivo* Detection of Hydroxyl Radical

Zhen Li,[†] Tao Liang,[†] Songwei Lv,[†] Qinggeng Zhuang,[‡] and Zhihong Liu*[,†]

[†]Key Laboratory of Analytical Chemistry for Biology and Medicine (Ministry of Education), College of Chemistry and Molecular Sciences, Wuhan University, Wuhan 430072, China

[‡]Department of Chemistry and Biochemistry, The Ohio State University, Columbus, Ohio 43210, United States

Supporting Information

ABSTRACT: The detection of •OH in live organisms is crucial to the understanding of its physiological and pathological roles; while this is too challenging because of the extremely low concentration and high reactivity of the species in the body. Herein, we report the rational design and fabrication of an NIR-light excited luminescence resonance energy transfer-based nanoprobe, which for the first time realizes the *in vivo* detection of •OH. The nanoprobe is composed of two moieties: upconversion nanoparticles with sandwich structure and bared surface as the energy donor; and mOG, a modified azo dye with tunable light absorption, as both the energy acceptor and the •OH recognizing ligand. The as-constructed nanoprobe exhibited ultrahigh sensitivity (with the quantification limit down to 1.2 femtomolar, several orders of magnitude lower than that of most previous •OH probes), good biocompatibility, and specificity. It was successfully used for monitoring [•OH] levels in live cells and tissues.

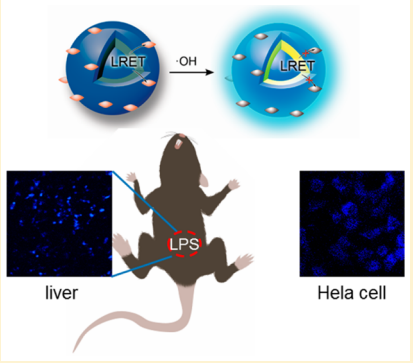

INTRODUCTION

Reactive oxygen species (ROS) have long been the focus of biological and medical studies due to their critical roles in numerous physiological and pathological processes, such as inflammation, cell signal transduction, and neurodegenerative diseases.[1−6] Hydroxyl radical (•OH) is one of the most reactive ROS, showing the strong ability to damage biomacromolecules including nucleic acids, proteins, lipids, and carbohydrates.[7−11] In order to properly understand the behaviors and functions of this vital species, it is crucial to determine •OH in live organisms with high specificity and sensitivity. However, the high reactivity and low *in vivo* concentration of •OH make it a very challenging task. Over the past decades, several techniques for the detection of •OH have been developed, which cover a wide range of methodology such as electron spin resonance (ESR) spectroscopy, chromatography, spectrophotometry, and electrochemical sensing.[12−17] But these methods are only suitable for *in vitro* •OH measurements. Considering the nondestructive and visual features, the fluorescence probe has been established as one of the most useful tools for real-time monitoring chemical species in live cells, tissues, and animals.[18−22] Indeed, several elegant fluorescence probes for •OH have previously been reported using either small-molecule or nanomaterial fluorophores.[23−27] Nonetheless, the use of these probes is somewhat limited due to the short excitation wavelengths in the UV−vis range, which suffers from shallow tissue penetration depths. Besides, the rather serious background interference in biological samples restricts the sensitivity of detection. For the above reasons, there has been no report on the *in vivo* detection of hydroxyl radical so far, hence it is still desired to create new probes for •OH with higher competence.

Upconversion nanoparticles (UCNPs), a kind of rare-earth ion doped luminophore excited with near-infrared (NIR) light, are particularly suitable for applications in biosensing and bioimaging because of the deeper tissue penetration and negligible autofluorescence from biomolecules under NIR excitation.[28−38] UCNPs are promising energy donors for luminescence resonance energy transfer (LRET)-based fluorescence probes, in which a specific target recognizing moiety acts as the energy acceptor and quenches the luminescence of UCNPs. The target-induced recovery of UCNPs luminescence can provide turn-on signals, with the sensitivity predominantly dependent on the quenching efficiency. Following this LRET principle, increasing amounts of UCNPs-based nanoprobes have been constructed for biologically relevant substances in live cells and tissues in these years.[39−45] Recently, a fluorescence probe for •OH using UCNPs as the energy donor was reported by Zhang et al.[46] Though delicately designed, this probe was however not able to monitor the low concentration of •OH *in vivo* because of the deficiency in energy transfer (represented by the quenching degree of the donor emission) and hence the insufficient sensitivity. As recognized, the energy-transfer efficiency is decided mainly with two factors, i.e., the donor-to-acceptor distance and the spectral match (the emission of energy donor and the absorption of energy acceptor). In our recent work, we reported a kind of

Received: July 5, 2015
Published: August 19, 2015

DOI: 10.1021/jacs.5b06972
J. Am. Chem. Soc. 2015, 137, 11179−11185

sandwich structured UCNPs (SWUCNPs for short), which provided largely shortened donor-to-acceptor distance and afforded significantly enhanced luminescence quenching degree of up to >80%, thus guaranteeing an improved signal-to-background ratio.[47] This consequence suggests the possibility of fabricating a highly sensitive nanoprobe for monitoring the extremely low levels of [•OH] by using SWUCNPs as the energy donor, combining a proper recognizing ligand for •OH with tunable light absorption. As such, it would be able to achieve the *in vivo* detection of hydroxyl radical.

RESULTS AND DISCUSSION

Design Principle of the LRET-Based •OH Nanoprobe. The design strategy of the probe relies on a LRET process from UCNPs to an energy acceptor mOG, as briefly depicted in Scheme 1. On one hand, we used the SWUCNPs ($NaYF_4$@$NaYF_4$:Yb,Tm@$NaYF_4$) with bared surface as the energy donors. This is to ensure that all emitting rare-earth ions are close enough to the recognizing ligand, which also functions as the energy acceptor, on the particle surface. On the other hand, an azo dye (mOG) responsive to •OH was designed as the ligand, which was assembled on the bared surface of SWUCNPs via the coordination between the carboxyl groups of mOG and the exposed lanthanide ions. The absorption band of mOG matches well with the emission of the SWUCNPs, resulting in LRET and quenching of the upconversion luminescence (UCL). Upon the reaction with •OH, mOG is oxidized and decomposed (the azo bond is broken by •OH). The light absorption of mOG is therefore altered, inhibiting the energy transfer from SWUCNPs to mOG. As a consequence, the UCL of SWUCNPs is recovered according to the amount of •OH, which allows quantitative detection of •OH.

Scheme 1. Principle of the Upconversion Nanoprobe for •OH Detection

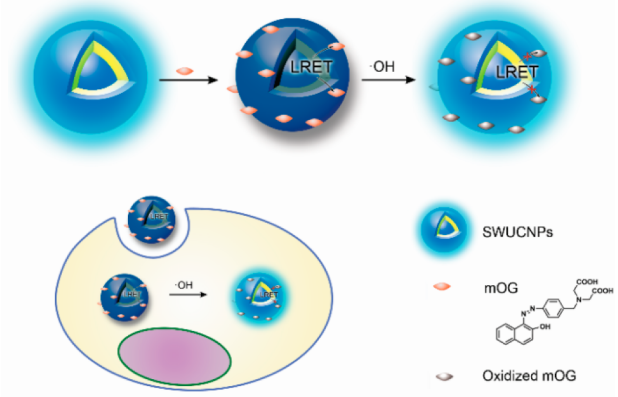

Optical Properties of mOG and Response to •OH. It is known that azo dyes typically show intense UV−vis absorption, which can be thoroughly eliminated when the molecules are degraded by •OH.[48−51] This provides the opportunity to sensitively modulate the spectral match between the energy donor and acceptor. We selected a commercially available dye Orange G (CAS 1936-15-8) as the starting material to synthesize mOG via a route shown in Figure S1.[52] Two carboxyl groups were tagged to the dye to coordinate with the lanthanide ions on the surface of the bared SWUCNPs (the NMR and MS characterizations of the molecule are shown in Figures S2−S4). mOG shows an intense absorption peak around 487 nm with a molar absorption coefficient of 1.5×10^4 L mol^{-1} cm^{-1} (Figure S5). The absorption band of mOG exactly matches with the blue emission of the SWUCNPs originating from the $^1G_4 \rightarrow {}^3H_6$ transition of Tm^{3+} under the excitation of 980 nm (Figure 1), which enables the energy

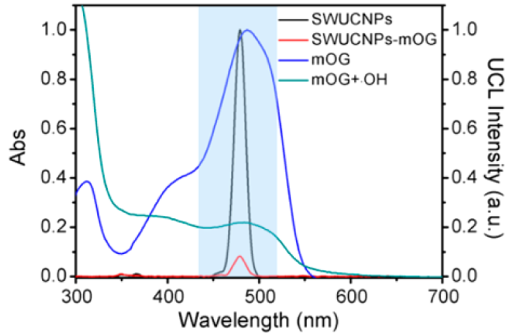

Figure 1. Emission of SWUCNPs matches well with the absorption band of mOG, but not that of oxidized product.

transfer from UCNPs to mOG and could lead to efficient quenching of the UCL. Figure 1 also reveals that the absorption of the dye in this region can be remarkably lowered after oxidation, which is essential to the inhibition of the energy-transfer process.

Properties of the Sandwich Structured UCNPs. The hexagonal-phase oleate-capped SWUCNPs with an average diameter of ∼33.1 nm (Figure 2) were synthesized using a layer-by-layer seed-mediated shell growth strategy according to our literature.[47] In a typical procedure, $NaYF_4$ nanocrystals were first synthesized as the core and subsequently coated with $NaYF_4$:Yb,Tm shell through the epitaxial growth. To protect the emitters from environmental quenching, another $NaYF_4$ shell was further deposited on the surface of the inner shell to form the SWUCNPs. The transmission electron microcopy (TEM) images illustrate the uniform size of the materials and its evolution (from the ∼23.6 nm $NaYF_4$ cores to the ∼29.3 nm $NaYF_4$@$NaYF_4$:Yb,Tm core−shell particles, and further to the ∼33.1 nm $NaYF_4$@$NaYF_4$:Yb,Tm@$NaYF_4$ sandwich particles) (Figure 2a−c). The high-resolution TEM (HRTEM) and selected-area electron diffraction (SAED) pattern (Figure 2e,f)

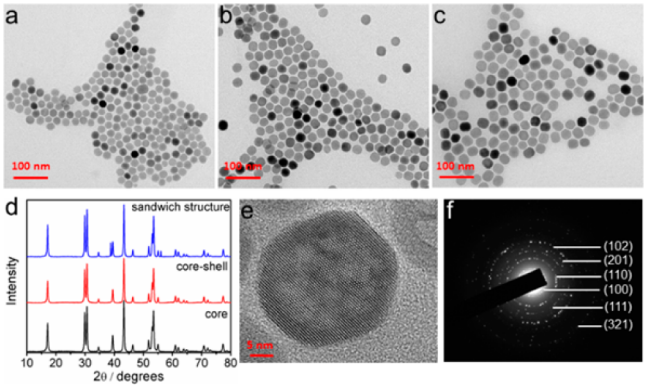

Figure 2. (a−c) TEM images of (a) $NaYF_4$, (b) $NaYF_4$@$NaYF_4$:Yb, Tm, (c) $NaYF_4$@$NaYF_4$:Yb,Tm@$NaYF_4$. (d) XRD patterns of the obtained nanocrystals. (e) HRTEM image and (f) SAED pattern of SWUCNPs indicate the obtained nanoparticles are with a hexagonal phase, which is consistent with the analysis of XRD.

DOI: 10.1021/jacs.5b06972
J. Am. Chem. Soc. 2015, 137, 11179−11185

show the spotty polycrystalline diffraction rings corresponding to the specific (100), (110), (111), (102), (201), (321) planes of the hexagonal-phase $NaYF_4$ lattice, which is consistent with the analysis of X-ray powder diffraction (XRD) (Figure 2d).

Fabrication of the mOG-SWUCNPs Nanoprobe. To assemble the SWUCNPs with mOG, the oleate ligands were removed by acid treatment to obtain water-dispersible bared SWUCNPs. The removal of oleate ligands was confirmed by Fourier transform infrared (FTIR) analysis, as presented by the weakening of the shoulder band at 2927 and 2852 cm^{-1} assigned to the asymmetric and symmetric stretching vibration of methylene ($-CH_2-$) in the long alkyl chain (Figure S6a). Furthermore, XRD patterns and TEM images indicate no significant effects on the crystalline phase, size, and shape of the nanoparticles during this acid treatment process (Figure S6b,c). The successful assembly of mOG on SWUCNPs surface was also confirmed by means of FTIR and ζ potential. After the attachment of mOG, the FTIR spectrum of the nanoparticles shows the band at 3000 cm^{-1} assigned to C−H stretching and the band at 1300 cm^{-1} attributed to stretching of the amino C−N bond. Meanwhile, the C═O stretching band at 1750 cm^{-1} disappears as the carboxyl groups coordinate to lanthanide ions (Figure 3a). The ζ potential of bared SWUCNPs was originally

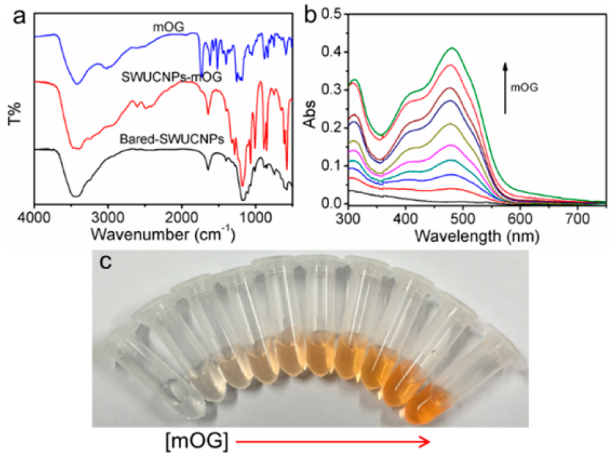

Figure 3. (a) FTIR spectra of mOG, mOG-SWUCNPs, and bared SWUCNPs. UV−vis spectra (b) and photographs (c) of SWUCNPs after assembly with different concentrations of mOG (ranging from 0 to 84.7 μM).

at +34 mV and shifted to +15 mV after mOG loading (Figure S7), which also indicates the binding of the dye to SWUCNPs. Another direct evidence of the fabrication of probe is the gradual increase of the absorption at 487 nm of the nanoparticles along with the increase of mOG concentration, which can even be observed with naked eyes (Figure 3b,c).

After assembly of mOG, the UCL of SWUCNPs was gradually quenched by increasing the amounts of mOG (Figure 4a). Owing to the perfect spectral overlap as well as the shortened donor-to-acceptor distance provided by the bared SWUCNPs, the luminescence of UCNPs was quenched by mOG to a degree of up to 90% (Figure 4b), which was acquired with 84.7 μM mOG loaded on 1.2 mg/mL SWUCNPs. This is a quite impressive luminescence quenching efficiency and was hardly reached in previously reported probes with upconversion nanocrystals as energy donors, ensuring considerably high signal-to-background ratio. As such, pronounced sensitivity can be expected in the subsequent target assay.

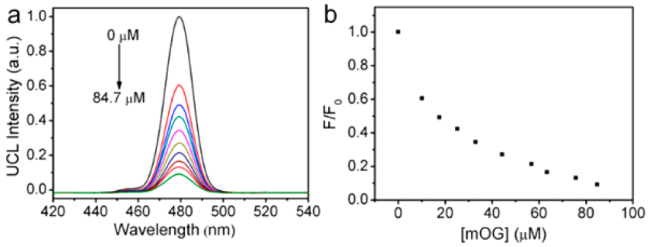

Figure 4. (a) Emission of SWUCNPs (1.2 mg/mL) loaded with different concentration of mOG. (b) Relative fluorescence intensity (F/F_0, in which F and F_0 represent the UCL emission intensity in the presence and the absence of mOG, respectively) of SWUCNPs after assembly of different concentrations of mOG.

Sensing of •OH with mOG-SWUCNPs in Aqueous Solution. We next examined the performance of this mOG-SWUCNPs nanoprobe for the determination of •OH, first in a buffered aqueous solution. •OH was generated through the photolysis of $NaNO_3$, a process that is able to produce •OH at femtomolar (fM) concentrations or lower, which are representative levels under biological conditions.[53−55] The absorption of mOG at 487 nm was reduced with increasing amount of •OH (Figure S8), as a result of the oxidation and decomposition of the azo dye. The concentration of •OH was controlled by adjusting the amount of $NaNO_3$ at constant time of irradiation by a mercury lamp. The relationship between •OH concentration and $NaNO_3$ concentration was determined by a method of kinetics of benzoate oxidation[55] (Figure S9). The as-generated •OH was calculated to be in the range of 1.2−194.6 fM with 0.5−200 mM $NaNO_3$, which is comparable to that reported by Pierre et al.[53] Obviously, the weakened absorption of mOG at 487 nm should disrupt the energy transfer from the energy donor to the acceptor. As a consequence, the luminescence of the SWUCNPs was recovered stepwise with adding increasing amounts of $NaNO_3$ (Figure 5a). More importantly, the UCL recovery of

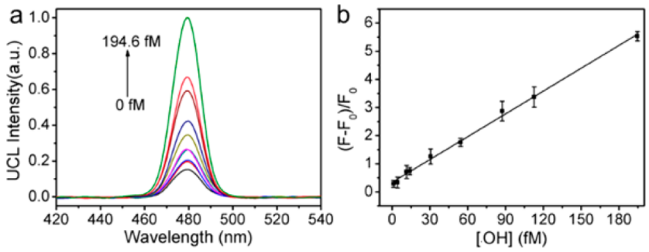

Figure 5. (a) UCL emission spectra of mOG-SWUCNPs in the presence of different concentrations of •OH (change the amount of $NaNO_3$ and give constant time of irradiation). (b) Relative fluorescence intensity ($(F - F_0)/F_0$) of the nanoprobe in response to varying concentration of •OH.

the SWUCNPs was dependent on the concentration of •OH, providing the opportunity to quantitatively detect •OH. As shown in Figure 5b, the relative fluorescence intensity of the probe ($(F - F_0)/F_0$, where F and F_0 represent the UCL intensity in the presence and the absence of •OH, respectively) is linearly correlated to the concentration of •OH in the range from 1.2 to 194.6 fM. Notably, the quantification limit of 1.2 fM is several orders of magnitude lower than that of most previous fluorescence probes for •OH. We also tested the response of the probe to •OH in another manner, where the

DOI: 10.1021/jacs.5b06972
J. Am. Chem. Soc. 2015, 137, 11179−11185

concentration of $NaNO_3$ was fixed with varying irradiation time. In this case, a linear increase in the UCL intensity was also observed (Figure S10), a result consistent with the literature.[53] Moreover, this upconversion nanoprobe displayed high selectivity to hydroxyl radical against other ROS, ions, small molecules, and proteins (Figure S11), which laid further foundation for the detection of •OH in complicated biological samples. Furthermore, the thermal stability and pH stability of the nanoprobe were investigated. Incubation of the nanoprobe at 37 °C for 2 h did not lead to significant variation in the signal (Figure S12a). Also, the emission intensity of the probe showed only a slight change in the range of pH 4.5−8.0 (Figure S12b). These results indicate excellent stability of the probe and its suitability for long-term observation in bioimaging.

Monitoring [•OH] in Live Cells. With the outstanding sensitivity and good specificity of the probe toward •OH in hand, we then investigated its biological applicability by monitoring intracellular •OH levels in live cells. Before bioimaging, we evaluated the cytotoxicity of the probe by the reduction activity of the methyl thiazolyl tetrazolium (MTT) assay. Following incubation of 0−0.6 mg/mL mOG-SWUCNPs for 24 h, the cell viability was >85% (Figure S13). A cell viability of >90% was maintained in the presence of 0.3 mg/mL probe, which is the amount we used in fluorescence microscopy experiments. UCNPs can be uptaken by cells via endocytosis, facilitated by dyneins.[56,57] In order to assess the uptake of the probe by live cells, we performed the single-cell Z-scanning experiment by confocal microscopy. Figure S14 shows that the nanoprobe can be efficiently uptaken into cells and evenly distributed in the cytosol, indicating satisfying biocompatibility of the probe. With the aim to detect the endogenously generated intracellular •OH, we designed three groups of HeLa cells for test. One group of cells was pretreated with 500 ng/mL phorbol myristate acetate (PMA), a stimulator of cell respiratory burst to give rise to ROS, followed by incubation with the nanoprobe for 1.5 h. In contrast to another group of cells untreated with PMA, an obvious increase of the UCNPs luminescence was observed after stimulation with PMA (Figure 6a,b). To confirm that the luminescence elevation was a result of the response of the probe to the generated •OH, a third group of cells was treated with 1.0 mM 2,2,6,6-tetramethylpiperidine-*N*-oxyl (TEMPOL) (a recognized radical scavenger) for 1 h before stimulation with PMA. It was found that the pretreatment with TEMPOL remarkably inhibited the luminescence of UNCPs (compare Figure 6c with 6b), firmly indicating that the alteration of probe signal is the reflection of intracellular [•OH] at different physiological situations. The quantitative intensities of UCL are integrated and compared in Figure 6d. These results have proven the ability of the mOG-SWUCNPs nanoprobe to detect intracellular •OH in live cells.

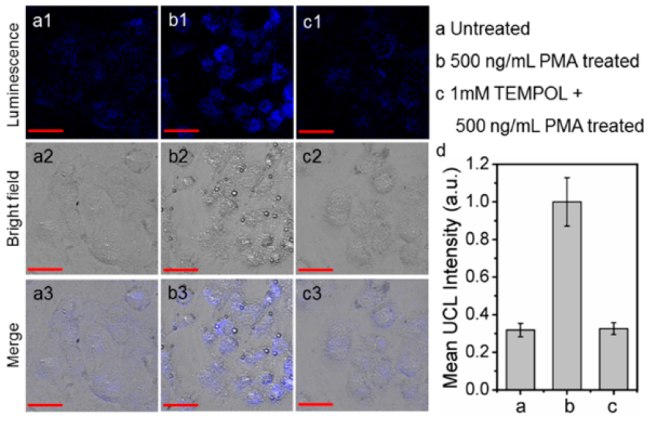

Figure 6. (a−c) Confocal microscopic images of HeLa cells incubated with the mOG-SWUCNPs nanoprobe (0.3 mg/mL): (a) cells incubated with the nanoprobe without pretreatment; (b) cells treated with 500 ng/mL PMA for 1 h before incubation with the nanoprobe; and (c) cells pretreated with TEMPOL for 1 h before stimulation with PMA. (d) Normalized average UCL intensities in (a−c). Images were collected at 450−500 nm. Scale bar: 30 μm.

***In Vivo* Detection of •OH in Mice Liver.** Ultimately, we attempted to apply this nanoprobe to the *in vivo* detection of •OH in mice liver. To this end, we used the probe to monitor the •OH levels in a lipopolysaccharide (LPS) model of acute inflammation. It was reported that the concentration of hydroxyl radical in organs increases due to the activation of macrophages and neutrophils in an LPS model.[58] We set altogether five batches of test samples, so as to obtain reliable results. For the first batch of sample, the mice were intraperitoneally (i.p.) injected with the nanoprobe (3.0 mg/100 g (body weight, same as below) in 300 μL of physiological saline). In this sample, we can observe a rather weak luminescence signal, which could be coming from the low level of intrinsic •OH in normal mice liver (Figure 7a,f). To confirm this, we tested a blank control where the mice were injected with only saline. In this case, the sample showed near-zero signal under NIR excitation (Figure 7e,f), which is also an evidence of the negligible autofluorescence of the biological sample. For the 3−5 batches of sample, the mice were injected with LPS at 1.0, 2.0, and 4.0 mg/100 g, respectively, before the injection of 3.0 mg/100 g nanoprobe. The luminescence intensities of these samples, as expected, are obviously higher than that of the above two groups. What's more, the intensity is corresponding to the amount of LPS injected (Figure 7b−d,f), which reveals the different levels of inflammation induced by the drug. These observations have demonstrated the capability of the as-constructed upconversion nanoprobe to monitor •OH in live tissues, which is by far the first successful example of *in vivo* •OH detection.

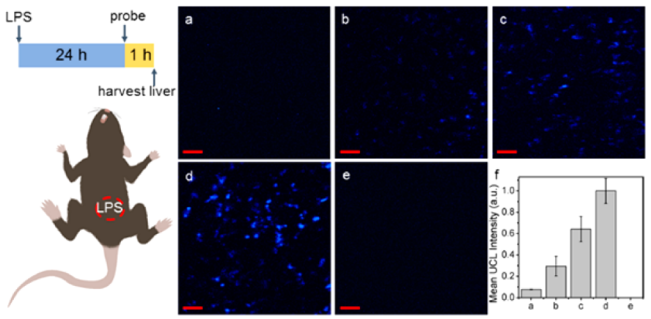

Figure 7. (a−e) UCL imaging of mouse liver slice. (a−d) Mice injected with LPS [a: 0 mg/100 g (body weight, same as below), b: 1.0 mg/100 g, c: 2.0 mg/100 g, d: 4.0 mg/100 g] 24 h before the injection of the nanoprobe. (e) Mice injected with physiological saline without the nanoprobe. (f) Normalized average UCL intensities in (a−e). Images were collected at 450−500 nm. Scale bar: 100 μm.

CONCLUSION

In summary, an NIR-light excited fluorescence probe for •OH has been developed for bioimaging in live organisms, using upconversion nanoparticles as the energy donors and the azo

DOI: 10.1021/jacs.5b06972
J. Am. Chem. Soc. 2015, 137, 11179−11185

dye mOG as the energy acceptor and specific recognition element. The rationally designed upconversion nanoprobe exhibits an excellent sensitivity for •OH with a quantification limit of 1.2 fM. It also shows high selectivity and stability, fine cellular uptake, and low cytotoxicity. The nanoprobe is able to monitor •OH in live cells and tissues owing to its favorable performances. This is the first probe capable of detecting the subtle variation of [•OH] *in vivo*, which may find broad applications in hydroxyl radical related biological and medical researches. The design strategy, which is uncomplicated and straightforward, can also be extended to develop other probes with high sensitivity for the *in vivo* detection of low-concentration substances.

EXPERIMENTAL SECTION

Synthesis of Modified Orange G (mOG). The synthetic routine of the azo dye mOG is shown in the Figure S1. Compound **2** was synthesized as reported.[52] 50 mg of **2** (0.20 mmol) was dissolved in the mixture of 0.5 mL of conc. HCl and 2 mL of H_2O in a round-bottomed flask and cooled in ice bath for 5 min. Then 2 mL of aqueous solution of $NaNO_2$ (13.8 mg, 0.20 mmol) was added to the solution with stirring dropwise. This solution was stirred for 1 h at 0 °C. Then **3** (28.8 mg, 0.20 mmol) in NaOH (aq) was added to yield orange-red precipitation. The mixture was stirred for another 1 h in ice bath.

Excess NaOH (aq) was added and stirred for another 4 h. Then excess HCl (1 N) was added and orange-red solid was formed. Compound **4** was obtained by filtration (25 mg, 37%). ^{1}H NMR (400 MHz, DMSO) δ 15.74 (s, 1H), 8.57 (d, J = 8.2 Hz, 1H), 7.96 (d, J = 9.4 Hz, 1H), 7.84 (d, J = 8.4 Hz, 2H), 7.80 (d, J = 7.9 Hz, 1H), 7.62 (t, J = 7.4 Hz, 1H), 7.53 (d, J = 8.3 Hz, 2H), 7.46 (t, J = 7.3 Hz, 1H), 6.95 (d, J = 9.4 Hz, 1H), 3.91 (s, 2H), 3.47 (s, 4H); ^{13}C NMR (101 MHz, DMSO) δ 172.70 (s), 167.71 (s), 145.07 (s), 139.92 (s), 133.13 (s), 130.51 (s), 129.54 (s), 129.46 (s), 129.30 (s), 128.25 (s), 126.15 (s), 123.99 (s), 121.75 (s), 119.62 (s), 57.18 (s), 54.17 (s); IR:1734, 1619, 1447, 837 cm^{-1}. HRMS (ESI) for $C_{21}H_{18}N_3O_5$ [M − H]$^-$: calcd for 392.12519; found 392.12421.

Synthesis of Oleate-Covered SWUCNPs. SWUCNPs stabilized with oleate were prepared by seed-mediated growth. Yb^{3+} and Tm^{3+} were doped in the second layer (inner shell) of the nanoparticles. $Y(oleate)_3$ (1 mmol) and NaF (20 mmol) were added to 10 mL of oleic acid/1-octadecene (OA/ODE, v/v = 1:1) and degassed at 110 °C in vacuum for 1 h in a three-neck flask. Then the mixture was kept at 320 °C in Ar atmosphere. An aliquot of 4 mL of the reaction mixture was withdrawn 75 min later and saved. 0.4 mmol of $Ln(oleate)_3$ (Y^{3+}:Yb^{3+}:Tm^{3+} = 79.8:20:0.2) in 8 mL of OA/ODE was added to the reaction. A second aliquot of 6 mL was taken 20 min later. 0.4 mmol of $Y(oleate)_3$ in 8 mL of OA/ODE was added to the reaction, which was then kept at 320 °C for another 20 min before cooled. All aliquots, including the final product solution, were mixed with equal volumes of ethanol at room temperature to precipitate the nanoparticles. Mixtures were centrifuged and washed six times with 1:1 hexane/ethanol. The first and second aliquots were the cores and the core−shell particles, respectively. The final product was SWUCNPs. All were capped by oleate.

Removal of Oleate. Bared SWUCNPs were obtained by treating oleate-covered SWUCNPs with acid. 60 mg of oleate-covered SWUCNPs were dispersed in 30 mL of HCl solution in ethanol (pH = 1.0). The solution was sonicated for 1 h. Bared particles were collected by centrifugation and washed with an HCl/ethanol solution at pH 4.0, followed by washing with ethanol and ultrapure water several times. Finally the product was redispersed in ultrapure water for storage.

Preparation of mOG-SWUCNPs. Bared SWUCNPs (1.2 mg) were mixed with 10−100 nmol of mOG in MOPS buffer (1.0 mL, 10 mM, pH = 7.2, with 100 mM KCl). The mixture was shaken gently overnight. The product was collected by centrifugation and washed with ultrapure water several times before being redispersed in MOPS buffer to a final concentration of 1.2 mg/mL.

Calculation of [•OH] Generated by $NaNO_3$ Photolysis. Initial concentration of benzoate was constantly 0.1 mM. Irradiation times ranged from 3 to 48 min. [$NaNO_3$] ranged from 0.5 to 200 mM. The steady-state concentrations of hydroxyl radical was determined by kinetics of benzoate oxidation, which follows rate equation $r = k_2$[•OH][benzoate]. Variable r stands for the rate of benzoate oxidation, and k is the rate constant. When hydroxyl radical is at steady state, [•OH] is regarded as constant, and the reaction becomes a pseudo-first-order reaction described by equation $r = k_1$[benzoate], where $k_1 = k_2$[•OH]. When the reaction is at the initial stage and only a small percentage of benzoate is consumed, the reaction can be treated as a pseudo-zero-order reaction described by $r = k_0$, where $k_0 = k_2$[•OH][benzoate]. Excited at 330 nm, the products of benzoate, mainly hydroxybenzoate, show a fluorescence peak at 450 nm. Solutions with constant [benzoate] and varing [$NaNO_3$] were irradiated with a UV lamp. Fluorescence spectra were scanned at time intervals from 3 to 20 min. Intensity at 450 nm was plotted over time and subject to either exponential (for pseudo-first-order) or linear fitting (for pseudo-zero-order). The second-order rate constant k_2 of benzoate was reported to be 5.9×10^9 M^{-1}·s^{-1}. [•OH] was then calculated based on k_2 and the result of experimental fitting.

***In vitro* Assay of •OH with mOG-SWUCNPs.** In pure water, 0.09 mg/mL mOG-SWUCNPs was mixed with various concentrations of $NaNO_3$ (0.5−200 mM) and irradiated with a mercury lamp for 90 min. UCL was then measured at 478 nm, excited with continuous-wave laser at 980 nm.

Selectivity of the Nanoprobe. In the control group, 0.09 mg/mL mOG-SWUCNPs were mixed with 200 mM $NaNO_3$ and irradiated with a mercury lamp for 90 min. In other groups, the mOG-SWUCNPs were incubated with interfering substances (200 mM for $NaNO_3$ and 10 μM for others). Then UCL was measured at 478 nm, excited with continuous-wave laser at 980 nm.

Stability of mOG-SWUCNPs Nanoprobe. To study the thermal stability, the mOG-SWUCNPs (0.09 mg/mL) were incubated at 37 °C, and UCL was recorded at given intervals for 2 h. Buffers with different pH were prepared by using citrate and phosphate salts. UCL signals of 0.09 mg/mL mOG-SWUCNPs in buffers were measured.

Cell Culture. HeLa cell lines were seeded in Dulbecco's modified Eagle's medium (DMEM) in a 24-well microplate with cover glasses, supplemented with 10% fetal bovine serum, 100 mg/L streptomycin, and 100 U/mL penicillin. The plate was then incubated for 24 h under 5% CO_2 at 37 °C.

Evaluation of Cytotoxicity. The cytotoxicity was evaluated by MTT assay. HeLa cells were cultured in DMEM in 96-well microplates at 37 °C under 5% CO_2 for 12 h. The medium was next replaced by fresh medium containing various concentrations of mOG-SWUCNPs (0−0.6 mg/mL). Each concentration was tested in three replicates. Cells were rinsed twice with phosphate buffer saline (PBS, pH = 7.2, with 137 mM NaCl, 2.7 mM KCl, 10 mM Na_2HPO_4 and 1.8 mM KH_2PO_4) 24 h later and incubated with 0.5 mg/mL MTT reagent for 4 h. DMSO was then added to dissolve formazan. The absorbance at 490 nm was measured in a microplate reader. Cell viability (%) was calculated according to following equation: Viability = (mean Abs. of treated wells/mean Abs. of control wells) × 100%.

Detection of Cytosol [•OH] in HeLa Cells. For labeling, the growth medium was removed and changed with serum-free DMEM. Then HeLa cells were incubated with mOG-SWUCNPs (0.3 mg/mL in serum-free DMEM) for 1.5 h under 5% CO_2 at 37 °C before being washed with PBS. The positive group was treated with PMA (500 ng/mL) for 1 h before incubation with mOG -SWUCNPs. To confirm the signal change was due to the response of probe to the generated hydroxyl radicals, another group of cells as contrast were treated with 1.0 mM TEMPOL for 1 h before stimulation with PMA. Images were captured with a Nikon Ni-E Microscope equipped with 980 nm laser.

Detection of [•OH] in Mice Liver. C57BL/6 mice (female, ~ 20 g) were i.p. injected with mOG-SWUCNPs (3 mg/100 g body weight in 300 μL of physiological saline). Three positive groups were i.p. injected with LPS (1.0, 2.0, 4.0 mg/100 g body weight in 200 μL of

DOI: 10.1021/jacs.5b06972
J. Am. Chem. Soc. 2015, 137, 11179−11185

saline) 24 h before the injection of mOG-SWUCNPs. Mice were sacrificed to harvest the livers 1 h after the injection of the nanoprobe. Livers were sliced and observed under microscope.

■ ASSOCIATED CONTENT

Supporting Information

The Supporting Information is available free of charge on the ACS Publications website at DOI: 10.1021/jacs.5b06972.

NMR, MS characterization and response to •OH of mOG, the XRD, TEM, FTIR characterization of SWUCNPs, the results of ζ potential measurements, the stability and cell viability of nanoprobe (PDF)

■ AUTHOR INFORMATION

Corresponding Author

*zhhliu@whu.edu.cn

Notes

The authors declare no competing financial interest.

■ ACKNOWLEDGMENTS

This work has been financially supported by the National Natural Science Foundation of China (no. 21375098, 21535005) and the National Basic Research of China (973 program, no. 2011CB933600).

■ REFERENCES

(1) Rhee, S. G. *Science* **2006**, *312*, 1882.
(2) Finkel, T.; Holbrook, N. J. *Nature* **2000**, *408*, 239.
(3) Branzk, N.; Lubojemska, A.; Hardison, S. E.; Wang, Q.; Gutierrez, M. G.; Brown, G. D.; Papayannopoulos, V. *Nat. Immunol.* **2014**, *15*, 1017.
(4) Strowing, T.; Henao-Mejia, J.; Elinav, E. *Nature* **2012**, *481*, 278.
(5) Wallace, D. C. *Science* **1999**, *283*, 1482.
(6) Xu, Q. L.; Heo, C. H.; Kim, G.; Lee, H. W.; Kim, H. M.; Yoon, J. *Angew. Chem., Int. Ed.* **2015**, *54*, 4890.
(7) Jacobs, A. C.; Resendiz, M. J. E.; Greenberg, M. M. *J. Am. Chem. Soc.* **2010**, *132*, 3668.
(8) Balasubramanian, B.; Pogozelski, W. K.; Tullius, T. D. *Proc. Natl. Acad. Sci. U. S. A.* **1998**, *95*, 9738.
(9) Malins, D. C.; Polissar, N. L.; Gunselman, S. J. *Proc. Natl. Acad. Sci. U. S. A.* **1996**, *93*, 2557.
(10) Yang, Y.; Zhao, Q.; Feng, W.; Li, F. *Chem. Rev.* **2013**, *113*, 192.
(11) Jiang, Y.; Zhao, H.; Lin, Y.; Zhu, N.; Ma, Y.; Mao, L. *Angew. Chem., Int. Ed.* **2010**, *49*, 4800.
(12) Scholz, F.; López de Lara González, G.; Machado de Carvalho, L.; Hilgemann, M.; Brainina, K. Z.; Kahlert, H.; Jack, R. S.; Minh, D. T. *Angew. Chem., Int. Ed.* **2007**, *46*, 8079.
(13) Huang, W.; Xie, W.; Luo, H.; Li, N. *J. Mater. Chem.* **2012**, *22*, 1477.
(14) Oka, T.; Yamashita, S.; Midorikawa, M.; Saiki, S.; Muroya, Y.; Kamibayashi, M.; Yamashita, M.; Anzai, K.; Katsumura, Y. *Anal. Chem.* **2011**, *83*, 9600.
(15) Xue, Y.; Luan, Q.; Yang, D.; Yao, X.; Zhou, K. *J. Phys. Chem. C* **2011**, *115*, 4433.
(16) Li, L.; Zhu, A.; Tian, Y. *Chem. Commun.* **2013**, *49*, 1279.
(17) Zhu, B.-Z.; Li, M.; Huang, C.-H.; Qin, H.; Fan, R.-M.; Kalyanaraman, B.; Zhu, J.-G. *Proc. Natl. Acad. Sci. U. S. A.* **2012**, *109*, 16046.
(18) Chang, M. C. Y.; Pralle, A.; Isacoff, E. Y.; Chang, C. J. *J. Am. Chem. Soc.* **2004**, *126*, 15392.
(19) Sasaki, E.; Kojima, H.; Nishimatsu, N.; Urano, Y.; Kikuchi, K.; Hirata, Y.; Nagano, T. *J. Am. Chem. Soc.* **2005**, *127*, 3684.
(20) Chan, J.; Dodani, S. C.; Chang, C. J. *Nat. Chem.* **2012**, *4*, 973.
(21) Lim, S. Y.; Hong, K. H.; Kim, D. I.; Kwon, H.; Kim, H. J. *J. Am. Chem. Soc.* **2014**, *136*, 7018.
(22) Ishida, M.; Watanabe, H.; Takigawa, K.; Kurishita, Y.; Oki, C.; Nakamura, A.; Hamachi, I.; Tsukiji, S. *J. Am. Chem. Soc.* **2013**, *135*, 12684.
(23) Zhuang, M.; Ding, C.; Zhu, A.; Tian, Y. *Anal. Chem.* **2014**, *86*, 1829.
(24) Yuan, L.; Lin, W.; Song, J. *Chem. Commun.* **2010**, *46*, 7930.
(25) Meng, L.; Wu, Y.; Yi, T. *Chem. Commun.* **2014**, *50*, 4843.
(26) Kim, M.; Ko, S. K.; Kim, H.; Shin, I.; Tae, J. *Chem. Commun.* **2013**, *49*, 7959.
(27) Song, Y.; Zhu, S.; Xiang, S.; Zhao, X.; Zhang, J.; Zhang, H.; Fu, Y.; Yang, B. *Nanoscale* **2014**, *6*, 4676.
(28) Wang, G.; Peng, Q.; Li, Y. *Acc. Chem. Res.* **2011**, *44*, 322.
(29) Achatz, D. E.; Ali, R.; Wolfbeis, O. S. *Top. Curr. Chem.* **2011**, *300*, 29.
(30) Zhou, J.; Liu, Q.; Feng, W.; Sun, Y.; Li, F. *Chem. Rev.* **2015**, *115*, 395.
(31) Liu, X.; Deng, R.; Zhang, Y.; Wang, Y.; Chang, H.; Huang, L.; Liu, X. *Chem. Soc. Rev.* **2015**, *44*, 1479.
(32) Dong, H.; Sun, L.; Yan, C. *Chem. Soc. Rev.* **2015**, *44*, 1608.
(33) Zheng, W.; Huang, P.; Tu, D.; Ma, E.; Zhu, H.; Chen, X. *Chem. Soc. Rev.* **2015**, *44*, 1379.
(34) Li, X.; Zhang, F.; Zhao, D. *Chem. Soc. Rev.* **2015**, *44*, 1346.
(35) Park, Y. I.; Lee, K. T.; Suh, Y. D.; Hyeon, T. *Chem. Soc. Rev.* **2015**, *44*, 1302.
(36) Chen, G.; Ågren, H.; Ohulchanskyy, T. Y.; Prasad, P. N. *Chem. Soc. Rev.* **2015**, *44*, 1680.
(37) Yang, D.; Ma, P.; Hou, Z.; Cheng, Z.; Li, C.; Lin, J. *Chem. Soc. Rev.* **2015**, *44*, 1416.
(38) Zhang, C.; Yuan, Y.; Zhang, S.; Wang, Y.; Liu, Z. *Angew. Chem., Int. Ed.* **2011**, *50*, 6851.
(39) Liu, J.; Liu, Y.; Bu, W.; Bu, J.; Sun, Y.; Du, J.; Shi, J. *J. Am. Chem. Soc.* **2014**, *136*, 9701.
(40) Peng, J.; Xu, W.; Teoh, C. L.; Han, S.; Kim, B.; Samanta, A.; Er, J. C.; Wang, L.; Yuan, L.; Liu, X.; Chang, Y. T. *J. Am. Chem. Soc.* **2015**, *137*, 2336.
(41) Xiao, Y.; Zeng, L.; Xia, T.; Wu, Z.; Liu, Z. *Angew. Chem., Int. Ed.* **2015**, *54*, 5323.
(42) Liu, Y.; Chen, M.; Cao, T.; Sun, Y.; Li, C.; Liu, Q.; Yang, T.; Yao, L.; Feng, W.; Li, F. *J. Am. Chem. Soc.* **2013**, *135*, 9869.
(43) Meier, R. J.; Simbürger, J. M. B.; Soukka, T.; Schäferling, M. *Anal. Chem.* **2014**, *86*, 5535.
(44) Li, L.; Wu, P.; Hwang, K.; Lu, Y. *J. Am. Chem. Soc.* **2013**, *135*, 2411.
(45) Chen, Z.; Liu, Z.; Li, Z.; Ju, E.; Gao, N.; Zhou, L.; Ren, J.; Qu, X. *Biomaterials* **2015**, *39*, 15.
(46) Mei, Q.; Li, Y.; Li, B.; Zhang, Y. *Biosens. Bioelectron.* **2015**, *64*, 88.
(47) Li, Z.; Lv, S.; Wang, Y.; Chen, S.; Liu, Z. *J. Am. Chem. Soc.* **2015**, *137*, 3421.
(48) Nango, M.; Iwasaki, T.; Takeuchi, Y.; Kurono, Y.; Tokuda, J.; Oura, R. *Langmuir* **1998**, *14*, 3272.
(49) Destaillats, H.; Turjanski, A. G.; Estrin, D. A.; Hoofmann, M. R. *J. Phys. Org. Chem.* **2002**, *15*, 287.
(50) Spadaro, J. T.; Isabelle, L.; Renganathan, V. *Environ. Sci. Technol.* **1994**, *28*, 1389.
(51) Maezono, T.; Tokumura, M.; Sekine, M.; Kawase, Y. *Chemosphere* **2011**, *82*, 1422.
(52) Morandeau, L.; Benoist, E.; Loussouarn, A.; Ouadi, A.; Lsaec, P.; Mougin, M.; Faivre-Chauvet, A.; Boterff, J. L.; Chatal, J. F.; Barbet, J.; Gestin, J. F. *Bioconjugate Chem.* **2005**, *16*, 184.
(53) Page, S. E.; Wilke, K. T.; Pierre, V. C. *Chem. Commun.* **2010**, *46*, 2423.
(54) Newton, G. L.; Milligan, J. R. *Radiat. Phys. Chem.* **2006**, *75*, 473.
(55) Buxton, G. V.; Greenstock, C. L.; Helman, W. P.; Ross, A. B. *J. Phys. Chem. Ref. Data* **1988**, *17*, 513.
(56) Dong, H.; Du, S.; Zheng, X.; Lyu, G.; Sun, L.; Li, L.; Zhang, P.; Zhang, C.; Yan, C. *Chem. Rev.* **2015**, DOI: 10.1021/acs.chemrev.5b00091.

DOI: 10.1021/jacs.5b06972
J. Am. Chem. Soc. 2015, 137, 11179−11185

(57) Bae, Y. M.; Park, Y. I.; Nam, S. H.; Kim, J. H.; Lee, K.; Kim, H. M.; Yoo, B.; Choi, J. S.; Lee, K. T.; Hyeon, T.; Suh, Y. D. *Biomaterials* **2012**, *33*, 9080.
(58) Kundu, K.; Knight, S. F.; Willett, N.; Lee, S.; Taylor, W. R.; Murthy, N. *Angew. Chem., Int. Ed.* **2009**, *48*, 299.

DOI: 10.1021/jacs.5b06972
J. Am. Chem. Soc. 2015, 137, 11179−11185